nature geoscience

LETTERS

PUBLISHED ONLINE: 15 AUGUST 2016 | DOI: 10.1038/NGEO2784

Palaeozoic oceanic crust preserved beneath the eastern Mediterranean

Roi Granot

Subduction of oceanic crust into the mantle results in the relatively young Mesozoic–Cenozoic age of the current oceanic basins[1], thus, hindering our knowledge of ancient oceanic lithospheres. Believed to be an exception, the eastern Mediterranean Sea (containing the Herodotus and Levant basins) preserves the southern margin of the Neotethyan, or older, ocean[2–4]. An exceptionally thick sedimentary cover[5] and a lack of accurate magnetic anomaly data have led to contradicting views about its crustal nature and age[2–9]. Here I analyse total and vector magnetic anomaly data from the Herodotus Basin. I identify a long sequence of lineated magnetic anomalies, which imply that the crust is oceanic. I use the shape, or skewness, of these magnetic anomalies to constrain the timing of crustal formation and find that it formed about 340 million years ago. I suggest that this oceanic crust formed either along the Tethys spreading system, implying the Neotethys Ocean came into being earlier than previously thought, or during the amalgamation of the Pangaea Supercontinent. Finally, the transition from the rather weak and stretched continental crust found in the Levant Basin[6–8] to the relatively strong oceanic Herodotus crust seems to guide the present-day seismicity pattern as well as the plate kinematic evolution of the region.

Remains of the ancient (>200 million years (Myr) ago) oceans are limited mostly to fragments preserved on land as ophiolite assemblages. However, the northeastern edge of the African Plate, located beneath the eastern Mediterranean Sea, has been suggested to preserve the remains of the southern Neotethys Ocean that formed as the Pangaea Supercontinent began to break apart along the northern Gondwana margin[2,10]. Constraints on the timing of Neotethys Ocean formation (Mediterranean sector) comprise stratigraphic, palaeontological and volcanological observations from along its margins indicating that deep-water seafloor spreading was already occurring by the middle Permian (~270 Myr ago)[3,11]. Alternatively, a recent global plate reconstruction model[4] predicted that the Mediterranean Sea may in fact preserve remnants of the early Devonian Palaeotethys Ocean. Thus far, however, remnants of these ancient oceans have never been identified in their original location. To some extent, the paucity of physical evidence is the result of the Mediterranean igneous crust being buried beneath an exceptionally thick sedimentary cover (>10 km), which has thus far precluded both the crustal nature (that is, oceanic versus continental crust) and the age from being definitively identified. As a result, the defining characteristics of the ancient seafloor spreading systems are clouded with uncertainty.

Onshore geologic observations from around the eastern Mediterranean suggest that the region was shaped through several extensional episodes[12] during the Permian, Triassic and Early Jurassic times. Ample evidence from deep seismic experiments[6,8] and gravity inversion[7] suggest that the easternmost part of the Mediterranean Sea (Levant Basin, Fig. 1) consists of stretched and thinned continental crust. Seismic data[5] and gravity inversion[7] from the Herodotus Basin, located west of the Levant Basin, suggest a gradual transition to a thinner, possibly oceanic crust. However, the sparse magnetic data from across the entire eastern Mediterranean appear, for the most part, to be non-coherent[9], an observation that has generated a long, ongoing debate as to the nature of these basins. Here I present 7,000 km of total field and vector magnetic profiles collected between 2012 and 2014 with a sea-surface towed system aboard the RV *Mediterranean Explorer* (Methods and Supplementary Fig. 1). In addition, I include total-field anomaly data from a 1998 well-navigated cruise on the RV *L'Atalante* (Fig. 1a) and use the recent version of the satellite altimetry-derived free-air gravity anomaly field[13] to highlight deeply buried crustal structures.

The collected total-field magnetic data reveal a previously undetected, spatially coherent sequence of anomalies in the eastern part of the Herodotus Basin with peak-to-trough amplitudes of ~100 nT (Fig. 1b). These long-wavelength anomalies, straddling 250 km along strike, form two sub-parallel NE–SW linear segments connected via a curved segment. The power spectra of these total-field anomalies (Supplementary Fig. 2) provide a crude, yet helpful estimate of the depth of the magnetic source layer, suggesting that it is situated about 13 to 17 km below the seafloor. This implies that the magnetic source layer underlies the sedimentary cover[5] and resides within the igneous crust.

Importantly, the lack of pronounced gravity anomalies in the Herodotus Basin (Fig. 1b) implies that the sequence of magnetic anomalies is not associated with lithological variations or prominent crustal structures (Supplementary Information and Supplementary Fig. 3), but rather, that they are caused by spatial variations in crustal magnetization. Thus, for the 250-km long, linear magnetic anomalies found in the Herodotus Basin to exist requires that the crust is oceanic, formed along segments of mid-oceanic ridge oriented in a NE–SW direction. In the centre of the curved sequence, the anomalies are highly reduced where they exhibit a small, 20-km left-stepping offset (black arrow in Fig. 1b). Outside this zone, the anomaly amplitudes gradually increase towards the offset. This pattern of amplitude enhancement towards the spreading offset has been observed in the Pacific[14], Atlantic[15] and Indian[16] oceans, in all three of which it was linked to end-of-segment enrichment of magnetite concentrations related to elevated magmatic fractionation and/or serpentinization. The long sequence of linear anomalies in the Herodotus Basin is located west of, and roughly parallel to, a gravity feature that is clearly depicted by the vertical gradient of the gravity field (Fig. 1b). Situated to the east of the gravity feature is the stretched continental crust of the Levant Basin[7,8], an observation indicating that the gravity feature probably marks the western boundary of the transition zone between the continental and oceanic crusts of the Herodotus Basin.

The full vector magnetic data independently confirm that a transition from oceanic to continental crust occurs between the

Department of Geological and Environmental Sciences, Ben-Gurion University of the Negev, Beer-Sheva 84105, Israel. e-mail: rgranot@bgu.ac.il

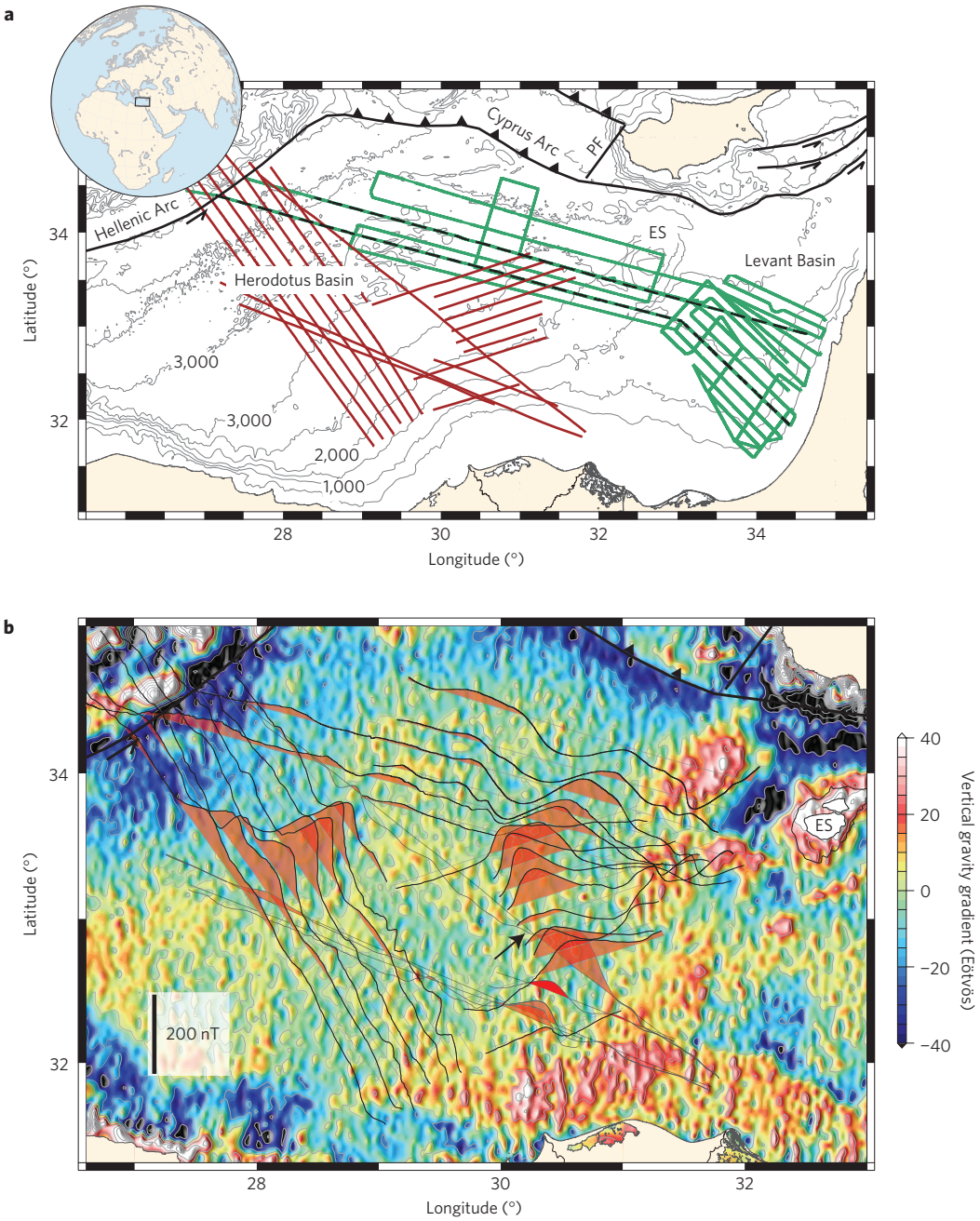

Figure 1 | Total-field magnetic anomalies in the Herodotus Basin. a, Tectonic map of the eastern Mediterranean. The green and brown lines show the tracks of the RV *Mediterranean Explorer* and the RV *L'Atalante*, respectively. Dashed black lines represent the vector profiles shown in Fig. 2. Grey lines delineate depth contours[28]. **b**, Total-field magnetic anomalies superimposed on a vertical gravity gradient map derived from satellite altimetry[13]. The magnetic anomalies are plotted along tracks. Red shading indicates positive anomalies. Black arrow shows the location of reduced anomalies. Abbreviations: ES, Eratosthenes Seamount; PF, Pafos Fault.

Herodotus and Levant basins, respectively. For a two-dimensional magnetic source layer (that is, oceanic crust located far from spreading offsets and/or secondary volcanic features), the horizontal and vertical components of the anomalies are phase-shifted by $\pi/2$, whereas for a three-dimensional source (that is, continental crust), the components are not coherently phase-shifted[17,18]. The horizontal component and the $\pi/2$ phase-shifted vertical component observed in the Herodotus Basin (Fig. 2 and Supplementary Fig. 4) generally resemble each other, confirming that the magnetic source layer is best characterized by a two-dimensional source structure. The components of the anomalies in the Levant Basin, in contrast, are non-coherent. The transition between the coherent and the non-coherent (that is, three-dimensional) data occurs along the positive gravity feature found between the Levant and Herodotus basins, a finding that further confirms its nature as the edge of the transition zone between two contrasting types of crust.

The lineated, total-field data contain a short sequence (across strike) of negative–positive–negative anomalies that cannot be uniquely correlated with the geomagnetic polarity timescale, and therefore, it is not possible to assign an accurate accretion age to the Herodotus crust. However, the mostly continuous northward and anticlockwise motion of the African Plate during the Palaeozoic and Mesozoic eras[19] resulted in predictable, age-dependent, crustal remanent magnetization directions. Assuming a simple magnetic source layer structure (that is, vertical magnetic boundaries), the shape (skewness) of the Herodotus magnetic anomalies depends

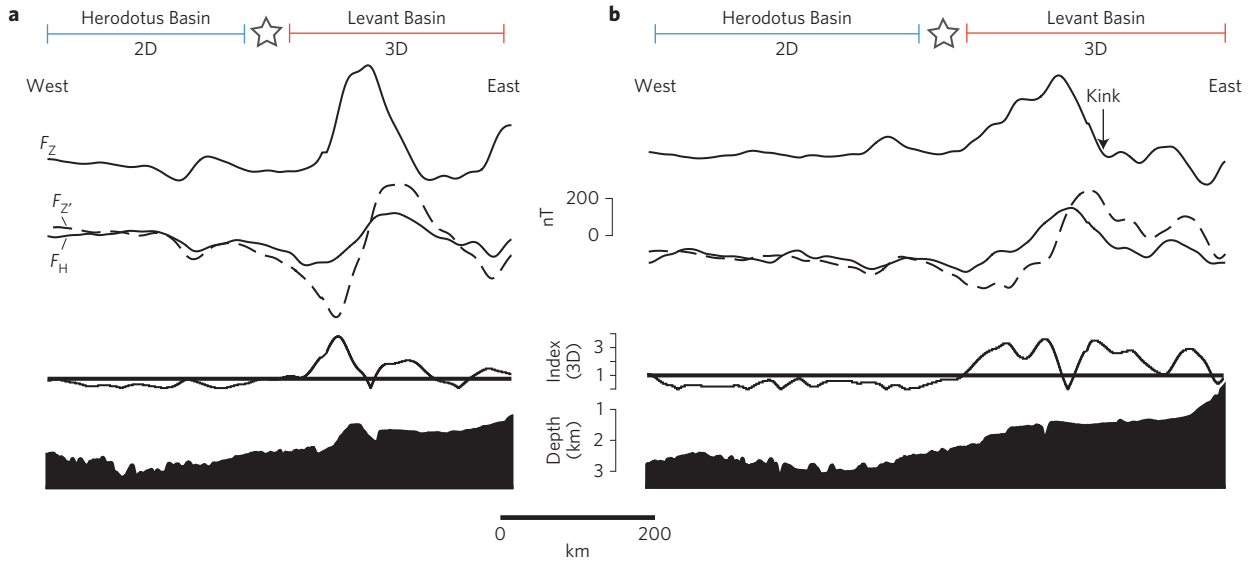

Figure 2 | Discrimination between two- and three-dimensional magnetic sources. a,**b**, Two representative vector profiles—northern (**a**) and southern (**b**), indicated by dashed lines in Fig. 1a—are shown with vertical (F_Z), horizontal (F_H), the $\pi/2$ phase-shifted vertical component ($F_{Z'}$, dashed line), and three-dimensional index and depth profiles. Abrupt transitions between two-dimensional magnetic sources (index < 1; ref. 18) and three-dimensional sources (index > 1) are marked by white stars at the top and projected in Fig. 4 and in Supplementary Fig. 4.

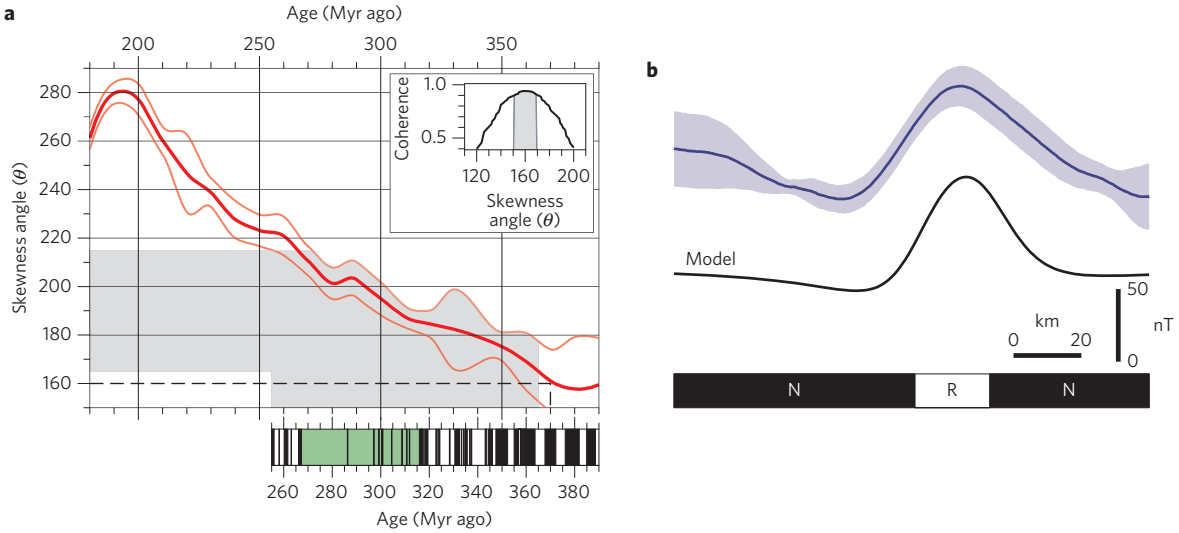

Figure 3 | Crustal age model. a, Expected skewness curve (red line shown with uncertainties as thin lines) for marine magnetic anomalies located on the northern African Plate (34° N, 30° E). The apparent polar wander path of Africa (and its α_{95} uncertainties)[19], with a magnetic boundary azimuth of 45°, was used to calculate the curve. The grey area represents the range of uncertainty of the observed skewness angles, corrected for anomalous skewness. The inset panel shows the coherence analysis of the de-skewed stacked anomalies (shown in **b**) against a reference polar (that is, zero skewness) forward magnetic anomaly model. The geomagnetic polarity timescale[22] is shown for the possible range of crustal ages (bottom). The green shading highlights the Kiaman Superchron. **b**, Stack (top, 8 profiles) of the total-field magnetic anomalies found in the eastern Herodotus Basin. A two-dimensional forward magnetic anomaly model (black line) assumes a flat magnetic layer between depths of 18.0 and 18.5 km with magnetization of 7 A m^{-1}. Other model parameters: $I_0 = 49°$; $D_0 = 4°$; azimuth = 45°. Remanence directions ($I_r = -64°$; $D_r = 19°$) are based on the 370 Myr African virtual geomagnetic pole[19].

on the present-day anomaly strike and geomagnetic field directions and the age-dependent remanent magnetization directions[20]. I constructed a time-dependent reference skewness curve (red curve in Fig. 3a) that I then used to estimate the crustal accretion age. I determined the skewness angle of the observed anomalies by comparing the de-skewed anomalies, using a range of possible angles, to a synthetic anomaly profile computed at the pole (that is, vertical magnetization and geomagnetic field directions). Best coherency (0.90 to 0.94, the range accounts for the 95% confidence bound) was achieved for a skewness angle of 160° ± 10° (Fig. 3a and Supplementary Fig. 5), which best fits the expected skewness angle calculated for 370 Myr-old crust. This calculation, however, does not account for possible anomalous skewness that is commonly observed at slow- to intermediate-spreading ridges[21], the likely range of spreading rates in a newly established spreading system[1]. Correcting the observed skewness for the appropriate anomalous skewness (30° ± 15°) (ref. 21) results in a corrected skewness angle of 190° ± 25° (the uncertainty is the sum of uncertainties related to skewness determination and anomalous skewness). Considering the uncertainties in the palaeogeography of the African Plate over time[19], the overall range of possible crustal age spans between 365 and 255 Myr ago (Fig. 3a). At least 200 km of the crust found in the

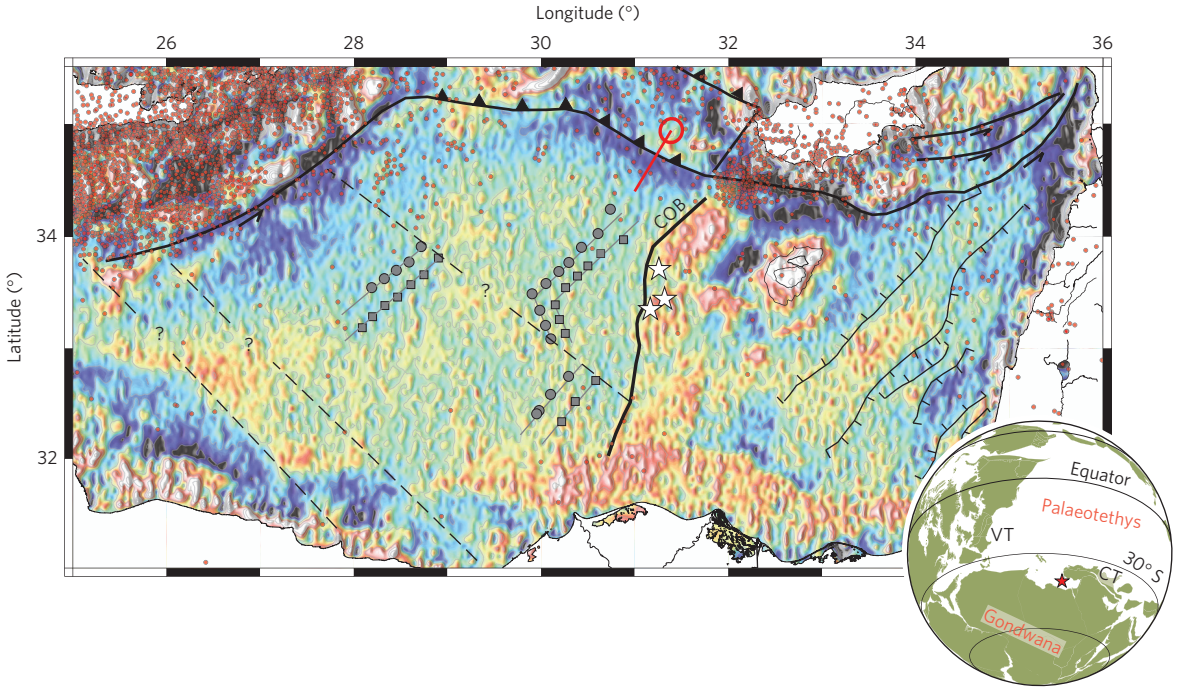

Figure 4 | Tectonic map of the eastern Mediterranean. Background is a VGG map[13]. Boundaries of basement highs in the Levant Basin are based on a Bouguer map (Supplementary Fig. 7) and on seismic data[29]. White-filled stars show the transition between two- and three-dimensional magnetic source layers computed along vector profiles (Supplementary Fig. 4). Grey-filled symbols denote isochrons. The dashed lines delineate the suspected location of fracture zones based on magnetic anomaly offsets and the background gravity grid. The motion of the Nubia Plate relative to that of the Anatolia Plate[30] is shown across the Cyprus arc with a red line (16.2 mm yr^{-1}). Red dots denote earthquake epicentres taken from the USGS catalogue with body wave magnitude (m_b) > 3 between 1972 and 2015. The inset panel shows the 340 Myr global palaeogeographic reconstruction[4]. Red star delineates the location of the Herodotus Ridge. Abbreviations: COB, continent–ocean boundary; VT, Variscan Terranes; CT, Cimmerian Terranes.

central and western parts of the Herodotus Basin is normally magnetized (Figs 3b and 4), which indicates that it must have formed during a normal polarity chron of the geomagnetic field. Assuming a reasonable range of half-spreading rates (50 km myr^{-1} or smaller), this normal chron lasted at least 4 Myr. The geomagnetic field during the Late Carboniferous to middle Permian[22] was dominated by the reversed Kiaman Superchron (Fig. 3a). Importantly, long (>2 Myr) normal geomagnetic chrons, within the range of the possible crustal ages, are known to have occurred only before 316 Myr ago. Therefore, I conclude that the estimated age of the Herodotus crust is 340 ± 25 Myr (that is, early to middle Carboniferous). I note, however, that because the palaeogeography of the African Plate during the Devonian and Carboniferous is loosely constrained[19], the older age bound is not well determined. Future palaeomagnetic data covering the Devonian to the Carboniferous periods will likely help reduce the uncertainty in the palaeogeography of the African Plate—which, in turn, will help refine the Herodotus crustal age.

The existence of Carboniferous oceanic crust in the Herodotus Basin has important regional geodynamic implications. The presence of a Palaeozoic NE–SW mid-ocean ridge system implies that the southern boundary of the Herodotus Basin, situated north of Egypt, functioned for the most part as a sinistral transform fault during the period that followed the initiation of seafloor spreading, when the Herodotus Ridge drifted westwards (Fig. 4). Motion along this transform boundary ceased once the ridge had drifted to the west, leaving the oceanic Herodotus crust juxtaposed against the African continental crust. A similar tectonic setting exists along many parts of the modern continental margins (for example, the St. Paul and Romanche fracture zones found in the Equatorial Atlantic). In addition, recent seismic observations[23] and gravity inversion[7] across the Egyptian margin indicate that the northern margin of Egypt was shaped by lateral motion.

The transition from the rather weak and stretched continental crust of the Levant Basin to the relatively strong oceanic crust of the Herodotus Basin created a mechanical boundary that may have influenced the location of the western boundary of the Sinai Microplate[24], which was formed during the Oligocene by the fragmentation of the northeastern part of the African Plate. In addition, seismic data from along the Cyprus arc (Fig. 4) reveal a dense cluster of earthquakes near the northwestern boundary of the Levant Basin that, just across the Pafos Fault to the west, abruptly transitions to diffuse activity. This shift may be the result of the transition between the continental collision occurring to the east and the subduction of the oceanic Herodotus crust beneath the Anatolian Plate to the west. Other factors (for example, seamounts and local crustal structures) may also contribute to shaping the observed earthquake pattern. However, a similar seismicity pattern is observed around the transition between the Zagros collision zone and the Makran subduction zone (Supplementary Fig. 6), supporting the causal link between the regional tectonic architecture and seismicity pattern.

The recognition of the NW–SE seafloor spreading in the eastern Mediterranean has important implications for the Carboniferous global plate tectonics. If the Herodotus Ridge was part of the Neotethyan spreading system, this implies that in the area of the Mediterranean Sea, the Neotethys Ocean came into being at least 50 Myr earlier than previously predicted[3,11], which, in turn, suggests that the Pangaea Supercontinent had already started to disperse before it completed its amalgamation at around 320 Myr ago[25]. Alternatively, the Herodotus spreading system may have been related to the older Palaeotethys spreading system. However, it seems unlikely that its opening was part of the Palaeotethys, which was active north of the Cimmerian Terranes[26] (Fig. 4), located between the present-day Turkey and Tibet. Instead, the opening along the Herodotus Ridge may have been unrelated to the Tethys spreading systems. For instance, the Herodotus crust may in fact expose part

of a back-arc basin associated with the final stages of amalgamation of the Pangaea Supercontinent and the formation of the Variscan orogeny[4,27]. These different tectonic scenarios should be tested using well-dated palaeomagnetic data constraining the motions of the different tectonic blocks surrounding the eastern Mediterranean.

Methods

Methods, including statements of data availability and any associated accession codes and references, are available in the online version of this paper.

Received 10 April 2016; accepted 8 July 2016; published online 15 August 2016

References

1. Müller, R. D., Sdrolias, M., Gaina, C. & Roest, W. R. Age, spreading rates, and spreading asymmetry of the world's ocean crust. *Geochem. Geophys. Geosyst.* **9,** Q04006 (2008).
2. Garfunkel, Z. Constraints on the origin and history of the Eastern Mediterranean basin. *Tectonophysics* **298,** 5–35 (1998).
3. Stampfli, G. M. & Borel, G. D. A plate tectonic model for the Paleozoic and Mesozoic constrained by dynamic plate boundaries and restored synthetic oceanic isochrons. *Earth Planet. Sci. Lett.* **196,** 17–33 (2002).
4. Domeier, M. & Torsvik, T. H. Plate tectonics in the late Paleozoic. *Geosci. Front.* **5,** 303–350 (2014).
5. de Voogd, B. *et al*. Two-ship deep seismic soundings in the basins of the Eastern Mediterranean Sea (Pasiphae cruise). *Geophys. J. Int.* **109,** 536–552 (1992).
6. Ben-Avraham, Z., Ginzburg, A., Makris, J. & Eppelbaum, L. Crustal structure of the Levant Basin, eastern Mediterranean. *Tectonophysics* **346,** 23–43 (2002).
7. Cowie, L. & Kusznir, N. Mapping crustal thickness and oceanic lithosphere distribution in the Eastern Mediterranean using gravity inversion. *Petrol. Geosci.* **18,** 373–380 (2012).
8. Netzeband, G. L. *et al*. The Levantine Basin—crustal structure and origin. *Tectonophysics* **418,** 167–188 (2006).
9. Rybakov, M., Goldshmidt, V., Hall, J. K., Ben-Avraham, Z. & Lazar, M. New insights into the sources of magnetic anomalies in the Levant. *Russian Geol. Geophys.* **52,** 377–397 (2011).
10. Stampfli, G., Marcoux, J. & Baud, A. Tethyan margins in space and time. *Palaeogeogr. Palaeoclimatol. Palaeoecol.* **87,** 373–409 (1991).
11. Stampfli, G. M. in *CROP PROJECT: Deep Seismic Exploration of the Central Mediterranean and Italy* (ed. Finetti, I. R.) 747–766 (Elsevier, 2005).
12. Garfunkel, Z. Origin of the Eastern Mediterranean basin: a reevaluation. *Tectonophysics* **391,** 11–34 (2004).
13. Sandwell, D. T., Müller, R. D., Smith, W. H. F., Garcia, E. & Francis, R. New global marine gravity model from CryoSat-2 and Jason-1 reveals buried tectonic structure. *Science* **346,** 65–67 (2014).
14. Granot, R., Cande, S. C. & Gee, J. S. The implications of long-lived asymmetry of remanent magnetization across the North Pacific fracture zones. *Earth Planet. Sci. Lett.* **288,** 551–563 (2009).
15. Pockalny, R. A., Smith, A. & Gente, P. Spatial and temporal variability of crustal magnetization of a slowly spreading ridge: mid-Atlantic ridge (20°–24° N). *Mar. Geophys. Res.* **17,** 301–320 (1995).
16. Hosford, A. *et al*. Crustal magnetization and accretion at the Southwest Indian Ridge near the Atlantis II fracture zone, 0–25 Ma. *J. Geophys. Res.* **108,** 2169 (2003).
17. Isezaki, N. A new shipboard three-component magnetometer. *Geophysics* **51,** 1992–1998 (1986).
18. Korenaga, J. Comprehensive analysis of marine magnetic vector anomalies. *J. Geophys. Res.* **100,** 365–378 (1995).
19. Torsvik, T. H. *et al*. Phanerozoic polar wander, palaeogeography and dynamics. *Earth Sci. Rev.* **114,** 325–368 (2012).
20. Schouten, H. & Cande, S. C. Paleomagnetic poles from marine magnetic anomalies. *Geophys. J. R. Astron. Soc.* **44,** 567–575 (1976).
21. Dyment, J., Cande, S. C. & Arkani-Hamed, J. Skewness of marine magnetic anomalies created between 85 and 40 Ma in the Indian Ocean. *J. Geophys. Res.* **99,** 24121–24134 (1994).
22. Ogg, J. G. in *The Geologic Time Scale 2012* (eds Gradstein, F. M., Ogg, J. G., Schmitz, M. D. & Ogg, G. M.) 85–114 (Elsevier, 2012).
23. Tari, G., Hussein, H., Novotny, B., Hannke, K. & Kohazy, R. Play types of the deep-water Matruh and Herodotus basins, NW Egypt. *Petrol. Geosci.* **18,** 443–455 (2012).
24. Salamon, A., Hofstetter, A., Garfunkel, Z. & Ron, H. Seismicity of the eastern Mediterranean region: perspective from the Sinai subplate. *Tectonophysics* **263,** 293–305 (1996).
25. Stampfli, G. M., Hochard, C., Vérard, C., Wilhem, C. & vonRaumer, J. The formation of Pangea. *Tectonophysics* **593,** 1–19 (2013).
26. Sengör, A. M. C. The Cimmeride orogenic system and the tectonics of Eurasia. *Geol. Soc. Am.* **195,** 1–82 (1984).
27. Pastor-Galán, D., Groenewegen, T., Brouwer, D., Krijgsman, W. & Dekkers, M. J. One or two oroclines in the Variscan orogen of Iberia? Implications for Pangea amalgamation. *Geology* **43,** 527–530 (2015).
28. Smith, W. H. F. & Sandwell, D. T. Global sea floor topography from satellite altimetry and ship depth soundings. *Science* **277,** 1956–1962 (1997).
29. Gardosh, M. A., Garfunkel, Z., Druckman, Y. & Buchbinder, E. in *Evolution of the Levant Margin and Western Arabia Platform Since the Mesozoic* (eds Homberg, C. & Bachmann, M.) 9–36 (Geol. Soc. Spec. Publ., 341, Geological Society of London, 2010).
30. Argus, D. F., Gordon, R. G. & DeMets, C. Geologically current motion of 56 plates relative to the no-net-rotation reference frame. *Geochem. Geophys. Geosyst.* **12,** Q11001 (2011).

Acknowledgements

I thank the captain, I. Katzman, of the RV *Mediterranean Explorer* and the entire staff of EcoOcean. Discussions with U. Barckhausen and M. Engels are greatly appreciated. This work was funded by the Israeli Ministry of Science, Technology and Space, grant 1151. The author was supported by the European Union Seventh Framework Program (FP7/2007–2013) under grant agreement 320496 (GEOPLATE) and the Israel Science Foundation grant 1844/12.

Additional information

Supplementary information is available in the online version of the paper. Reprints and permissions information is available online at www.nature.com/reprints.

Competing financial interests

The author declares no competing financial interests.

Methods

Magnetic anomaly data were collected aboard the RV *Mediterranean Explorer* during four cruises (MEDMAG Project) between 2012 and 2014. Data were collected using a towed system that included two total-field Overhauser sensors (Marine Magnetics SeaSpy) set up in longitudinal gradiometer mode (150 m spacing) and a third towfish mounted midway between the Overhauser sensors (Supplementary Fig. 1). The middle towfish contained a ringcore three-axial fluxgate magnetometer (Magson, resolution of 0.006 nT) and two tiltmeters (abj, resolution of 0.001°) that were used to constrain the pitch and roll angles. For the study area, where the strength of the ambient field is ~44,000 nT, the resultant resolution of the vertical component of the magnetic field is ~1 nT. Data were recorded at a sampling rate of 10 Hz. The magnetic data were integrated with the ship navigation data using the time stamps. Measurement positions were corrected to account for the towing cable lengths.

The processing scheme for the vector data follows ref. 31. Each of the three magnetic components of the vector data was calibrated to account for non-orthogonality, scale factors and gains. These nine parameters were first determined based on laboratory experiment, and refined for each cruise to account for variation in temperatures using data collected during calibration loops. Additionally, the tiltmeters were calibrated in the laboratory to account for nonlinearity response and misalignments with the three-axial magnetometer. During the first cruise, the r.m.s. differences along the calibration loop between the amplitudes of vector data and the total-field Overhauser data were 53.0 nT before calibration and reduced to 1.3 nT after calibration. Similar r.m.s. values were calculated for all four cruises. The three calibrated components were transformed to geographical coordinates using the corrected pitch and roll angles. Because the yaw angle was not directly measured and the variability of the water currents in the survey area is large, with apparently a range of wavelengths similar to that of crustal magnetic anomalies, it was not possible to reconstruct the yaw angle, and therefore the northern and eastern magnetic components, without introducing large errors. Hence, only the vertical and horizontal components were further considered in this study. Finally, the data were reduced to anomalies based on IGRF model 12 (ref. 32). The total-field magnetic anomalies were computed using the gradiometer data. The degree to which the external fields contributed to the signal was verified using data collected by the magnetic station located in Bar-Giora, Israel.

Code availability. The computer codes associated with this paper are available on request (rgranot@bgu.ac.il).

Data availability. The MEDMAG magnetic data are available through the National Geophysical Data Center (NGDC, https://www.ngdc.noaa.gov/mgg).

References

31. Engels, M., Barckhausen, U. & Gee, J. S. A new towed marine vector magnetometer: methods and results from a Central Pacific cruise. *Geophys. J. Int.* **172,** 115–129 (2008).
32. Thébault, E. *et al*. International Geomagnetic Reference Field: the 12th generation. *Earth Planets Space* **67,** 67–79 (2015).